

Efficient Star Distillation Attention Network for Lightweight Image Super-Resolution

Fangwei Hao, Ji Du, Desheng Kong, Jiesheng Wu, Jing Xu, *Member, IEEE*,
Ping Li, *Member, IEEE*

Abstract—In recent years, the performance of lightweight Single-Image Super-Resolution (SISR) has been improved significantly with the application of Convolutional Neural Networks (CNNs) and Large Kernel Attention (LKA). However, existing information distillation modules for lightweight SISR struggle to map inputs into High-Dimensional Non-Linear (HDNL) feature spaces, limiting their representation learning. And their LKA modules possess restricted ability to capture the multi-shape multi-scale information for long-range dependencies while encountering a quadratic increase in the computational burden with increasing convolutional kernel size of its depth-wise convolutional layer. To address these issues, we firstly propose a Star Distillation Module (SDM) to enhance the discriminative representation learning via information distillation in the HDNL feature spaces. Besides, we present a Multi-shape Multi-scale Large Kernel Attention (MM-LKA) module to learn representative long-range dependencies while incurring low computational and memory footprints, leading to improving the performance of CNN-based self-attention significantly. Integrating SDM and MM-LKA, we develop a Residual Star Distillation Attention Module (RSDAM) and take it as the building block of the proposed efficient Star Distillation Attention Network (SDAN) which possesses high reconstruction efficiency to recover a higher-quality image from the corresponding low-resolution (LR) counterpart. When compared with other lightweight state-of-the-art SISR methods, extensive experiments show that our SDAN with low model complexity yields superior performance quantitatively and visually.

Index Terms—Lightweight image super-resolution, Residual star distillation module, Multi-shape multi-scale large kernel attention module, Efficient star distillation attention network.

I. INTRODUCTION

Reconstructing a high-resolution (HR) image from corresponding low-resolution (LR) one is the goal of single image super-resolution (SR), a fundamental task in low-level vision. It has drawn the interest of numerous researchers during the last ten years, and significant progress has been made in this field. Many CNN-based methods have been put forth to continuously improve reconstruction performance, since Dong et al. [1] first design a three-layer super-resolution convolutional neural network named SRCNN, which achieves surprising performance than the conventional interpolation method [2]. A 20-layer network called VDSR is created by Kim et al. [3], and it outperforms SRCNN in terms of effectiveness

and demonstrates that one SR model's reconstruction performance can be enhanced by merely deepening the network. Following the residual learning [4], Lim et al. [5] develop an improved deep residual network (EDSR) by introducing the residual mechanism into one SR model. Although it results in significant reconstruction performance, the EDSR model is quite heavy. Next, based on residual mechanism and dense connection [6], Zhang et al. develop a residual dense network (RDN) [7] and a residual channel attention network (RCAN) [8], both of which are made up of hundreds of convolutional layers. While these are effective SR methods, they are opposed by significant computational loads and massive parameters, hindering their further applications on portable devices with limited computing resource. Therefore, designing lightweight and effective SR networks is essential.

In terms of lightweight SR, many recent CNN-based methods cope with this task by designing or borrowing advanced architectures or units. Concretely, Tai et al. [9] present the deeply-recursive residual network (DRRN), which is derived from the deeply-recursive convolutional network (DRCN) [10]. By sharing weights throughout the network, both networks reduce the model parameters. Such a parameter-sharing strategy results in a significant drop in model performance even though it reduces the model complexity. Additionally, other lightweight SR methods [11], [12], [13] based on feature distillation strategy are proposed. While the feature distillation strategy is effective for lightweight SR, the reconstruction performance and model efficiency of these distillation SR networks are slightly improved over DRRN, indicating that they are not efficient enough. More recently, PFFN [14] adopts pyramid spatial-adaptive feature extraction module (PSAFEM) and the enhanced channel fusion module (ECFM) to balance computational cost and performance, yet it produces restricted performance gain due to the lack of representative long-range dependencies. CFDM [15] improves prominent feature distillation network by incorporating convolutional modulation (Conv2Former) with dilated convolution to optimize network performance. However, implementing information distillation in low-dimensional spaces prevents it from achieving discriminative representation learning, resulting in limited reconstruction performance. The similar result is also encountered by FIWHN [16] that combines CNN and Transformer to explore a novel architecture which applies wide-residual distillation interaction blocks (WDIBs) with mutual information shuffle and fusion. Besides, HCFormer [17] utilizes a hybrid convolution-Transformer architecture which consists of lightweight and efficient convolution blocks (LECB) for

Fangwei Hao, Ji Du, Desheng Kong, Jiesheng Wu, and Jing Xu are with the College of Artificial Intelligence, Nankai University, Tianjin, 300350, China. Ping Li are with the Department of Computing, Hong Kong Polytechnic University, 999077, Hong Kong, China.

First Author and Second Author contribute equally to this work.

potential super-resolution features, and lightweight and efficient Transformer blocks (LETB) for long-term dependency. Nevertheless, they neglect to capture representative contextual information, leading to insufficient reconstruction efficiency. The same limitation goes for the OSFFNet [18] which develops an Omni-Stage Feature Fusion (OSFF) architecture to integrate features from different levels and capitalize on their mutual complementarity.

In addition, attention mechanism [19] is a common paradigm used in deep learning, and it is rapidly developed in convolutional neural networks and applied to various computer vision tasks, including image classification [20], [21], [22], [23], [24], [25], object detection [26], [27], [28], [29], semantic segmentation [30], [31], [32], [33], [34], and image restoration [35], [36], [37], [38], [39]. Recently, VAN [40] develops a large kernel attention (LKA) module by decomposing a large-kernel convolution into a small-kernel depth-wise convolution, a small-kernel depth-wise dilation convolution, and a point-wise convolution. LKA facilitates the learning for long-range dependencies which significantly improve the SR reconstruction performance. However, the computational and memory footprints of depth-wise convolutional layers in LKA rise quadratically as the size of the convolutional kernels increases. The same issue is encountered by LKDN [39], LKASR [37] or MSID [38] which employ LKA or scalable large kernel attention (SLKA) for lightweight SR task. To alleviate their complexity, Hao et al. [41] introduce a large separable kernel attention (LSKA) module [25] into lightweight SR task and propose a large coordinate attention network (LCAN). Although their LCAN achieves an effective reconstruction performance with low model complexity, it ignores the learning of multi-shape multi-scale information for long-range dependencies, resulting in limited performance on the public SR datasets.

Overall, existing lightweight image SR methods still show considerable potential for improvement of reconstruction efficiency. In particular, the prominent lightweight information distillation networks are executed in low-dimensional spaces, limiting their SR performance. Besides, existing CNN-based LKA and its improved versions either neglect to learn the multi-shape multi-scale information for long-range dependencies, or incur high computational and memory footprints with increasing convolutional kernel size of its depth-wise convolutional layer.

This paper aims at improving the information distillation ability of CNNs and capturing effective multi-shape multi-scale long-range dependencies, presenting a powerful efficient Star Distillation Attention Network (SDAN) for efficient lightweight SISR. SDAN consists of the proposed Star Distillation Module (SDM) and effective Multi-shape Multi-scale Large Kernel Attention (MM-LKA) module. Specifically, to improve the performance of information distillation modules, SDM is designed to enhance the learning for discriminative representation via information distillation in the high-dimensional non-linear (HDNL) feature spaces. Furthermore, MM-LKA module is developed to learn representative long-range dependencies which further boost the performance of CNN-based self-attention significantly. Additionally, we inte-

grate the proposed SDM, MM-LKA with residual structure [4] to generate a residual star distillation attention module (RSDAM) as the building block of our SDAN.

Our contributions are mainly four-fold:

- We propose an efficient Star Distillation Attention Network (SDAN) which possesses high reconstruction efficiency to recover a high-resolution (HR) image from the corresponding low-resolution (LR) one for lightweight SR.
- We present a Star Distillation Module (SDM) to enhance the learning for discriminative representation via information distillation in the HDNL feature spaces, and propose a Multi-shape Multi-scale Large Kernel Attention (MM-LKA) module to learn representative long-range dependencies.
- We develop a Residual Star Distillation Attention Module (RSDAM) by integrating the proposed SDM and MM-LKA, and take it as the building block of the proposed SDAN.
- The conducted extensive experiments show that our SDAN with low model complexity achieves superior performance quantitatively and visually, compared with other state-of-the-art lightweight SR methods.

II. RELATED WORK

A. Lightweight SR networks

Deep learning-based image super-resolution has advanced substantially in recent years. The groundbreaking SRCNN, a three-layer convolutional neural network (CNN) which can directly model the mapping function from LR to the corresponding HR, is first proposed by Dong et al. [1]. When compared to the earlier interpolation-based method [2], SRCNN demonstrates a significant improvement both quantitatively and visually because of CNN's powerful learning ability. Kim et al. [3] develop a very deep super-resolution (VDSR) network with 20 convolutional layers in order to improve performance even more. Next, by adopting the basic recursive structure, Kim et al. [10] present a deep recursive convolutional network (DRCN) to utilize fewer parameters for large receptive field. A deep recursive residual network (DRRN), an enhanced version of DRCN, is later proposed by Tai et al. [9]. DRRN performs better than DRCN with the same network depth yet fewer parameters. By integrating the group convolutions and the cascading technique, Ahn et al. [42] propose CARN, which makes a trade-off between computation complexity and model performance. Subsequently, Luo et al. [39] develop a lightweight SR model called LatticeNet that has comparatively low compute and memory requirements by economically adopting two butterfly structures to combine two residual blocks. Neural architecture search (NAS) technique, which enriches network structures, automatically constructs lightweight SR networks [43], [44]. Additionally, CNN-based feature distillation via dimension reduction or channel splitting is another effective strategy. Concretely, Hui et al. [11] first apply the feature distillation strategy to the SR task and present a lightweight information distillation network (IDN). IDN possesses quick execution because it uses group convolution

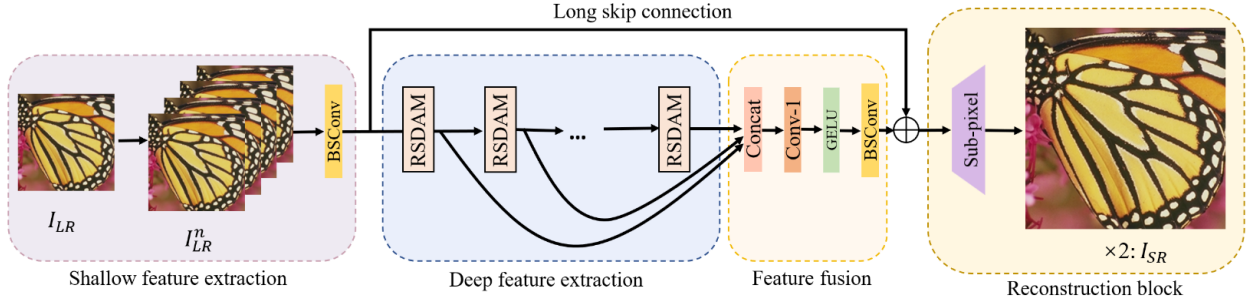


Fig. 1: Network architecture of our SDAN for $\times 2$ SR.

and has very few filters per layer. Furthermore, Hui et al. [12] improve IDN and propose a lightweight information multi-distillation network (IMDN) by building cascaded information multi-distillation blocks (IMDB), in which the channel splitting strategy is applied multiple times and the channel-wise attention mechanism is introduced. And IMDN takes the first place in the AIM 2019 constrained image SR challenge [45] due to its outstanding performance. Then, by combining the proposed feature distillation block with shallow residual connection, Liu et al. [13] further develop a residual feature distillation network (RFDN) based on IMDN, and it achieves effective performance while being more lightweight. More recently, in order to balance computational cost and model performance, PFFN [14] has adopted the enhanced channel fusion module (ECFM) and pyramid spatial-adaptive feature extraction module (PSAFEM), yet it only yields modest performance gains. To improve SR performance, CFDN [15] improves the prominent feature distillation network by incorporating convolutional modulation (Conv2Former) with dilated convolution. Its implementation of information distillation in low-dimensional spaces, however, hinders its efficiency and results in suboptimal reconstruction performance. FIWHN [16] employs wide-residual distillation interaction blocks (WDIBs) with mutual information shuffle and fusion for representative learning, and it mixes CNN and Transformer to explore a novel architecture. Besides, a hybrid convolution-Transformer architecture is also used by HCFormer [17], which comprises lightweight and efficient Transformer blocks (LETB) for long-term dependency, and lightweight and efficient convolution blocks (LECB) for potential super-resolution features. In addition, OSFFNet [18] develops an Omni-Stage Feature Fusion (OSFF) architecture to integrate features from different levels and capitalize on their mutual complementarity.

B. Vision attention

Viewed as an adaptive reweighting based on its input feature, vision attention has proven to be effective in both low-level tasks (e.g., image SR [36], [37], [38], [39], [40], [41], [46]) and high-level tasks (e.g., image classification [20], [21], [22], [23], [24], [25], object detection [26], [26], [27], [28], [29], [30], segmentation [31], [32], [33], [34]). The channel attention mechanism is first proposed in [20]. After demonstrating its efficacy in image classification, it and its modified versions [47], [48] are quickly adopted and utilized in SR networks [8], [49], [50]. The channel attention mechanism

presents notable gains in reconstruction performance with just refining the feature maps along the channel dimension. Recently, by decomposing a large-kernel convolution into a small-kernel depth-wise convolution, a small-kernel depth-wise dilation convolution, and a point-wise convolution, VAN [51] has developed a powerful large-kernel attention (LKA) module. LKA can effectively learn long-range dependencies which greatly enhance the performance of SR reconstruction. Nonetheless, as the size of the convolutional kernel rises, the memory and computing footprints of depth-wise convolutional layers in LKA increase quadratically. LKASR [40] develops a scalable large kernel attention (SLKA) which helps to improve the performance of lightweight SR. In order to reduce the complexity of LKA, Lau et al. [25] propose a family of large separable kernel attention (LSKA) for high-level tasks (e.g., image classification), by decomposing the two-dimensional (2D) convolutional kernels of the depth-wise convolutional layers in LKA into cascaded one-dimensional (1D) horizontal and vertical kernels, which incurs lower computational complexity. Hao et al. [52] further introduce LSKA into lightweight SR task and propose a large coordinate kernel attention network (LCAN) which shows remarkable performance. The success of these LKA-based SR methods indicates the importance of long-range dependencies for reconstruction.

III. METHODOLOGY

In this section, the overall network architecture of our SDAN is presented at first, followed by the detailed introduction of the proposed star distillation module (SDM). Next, we introduce the multi-shape multi-scale large kernel attention (MM-LKA) module. Subsequently, we provide the details about the residual star distillation attention module (RSDAM). Finally, the loss function is introduced in detail.

A. Network architecture

As Figure 1 shows, similar to previous lightweight SR works [13], our SDAN is primarily composed of four components: the shallow feature extraction part, residual star distillation attention modules (RSDAMs) for deep feature extraction, the feature fusion component, and the reconstruction block. Let I_{LR} represent the input Low-Resolution (LR) image, and I_{SR} denote the output of our SDAN. Initially, we duplicate the input image n times and stack them along the channel dimension. The resulting outcome, denoted as I_{LR}^n , serves as

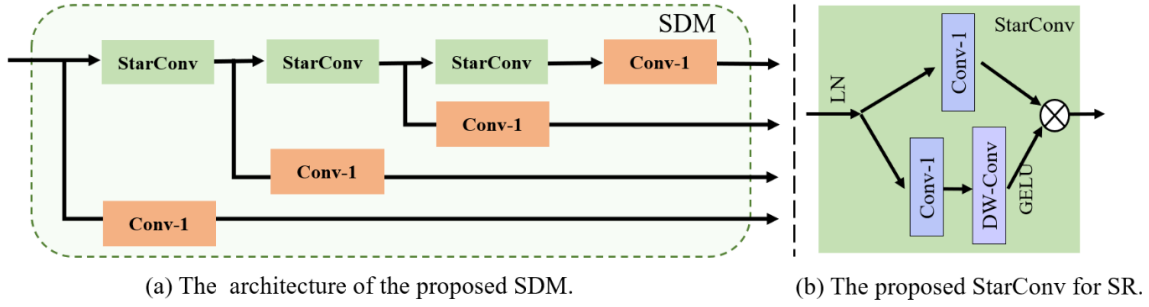


Fig. 2: The details of the proposed StarConv for high-dimensional mapping and star distillation module (SDM) for lightweight SR.

the input to the network. Then, we use only one BSConv layer as the shallow feature extraction part to extract the shallow feature F_0

$$F_0 = H_s(I_{LR}^n), \quad (1)$$

where $H_s(\cdot)$ is the BSConv operation. Subsequently, the obtained feature F_0 undergoes gradual refinement processes through M stacked residual star distillation attention modules (RSDAMs). The refined output feature generated by the last RSDAM represents the deep feature that has been effectively processed during the deep feature extraction part. Consequently, we can express the deep feature extraction process as

$$F_{\text{RSDAM}}^k = H_k(F_{\text{RSDAM}}^{k-1}), k = 2, \dots, M, \quad (2)$$

where $H_k(\cdot)$, F_{RSDAM}^{k-1} , and F_{RSDAM}^k are the k -th RSDAM operation, its input feature, and its output feature, respectively. After being progressively refined by M RSDAMs, we concatenate the obtained M intermediate features from M RSDAMs along the channel dimension, followed by one 1×1 convolution layer which is utilized to fuse the concatenated features, and a GELU [48] function for activation. Then, one 3×3 convolution layer is adopted to smooth the fused features. We can express the process as

$$F_{\text{fused}} = H_{\text{fusion}}(\text{Concat}(F_{\text{RSDAM}}^1, \dots, F_{\text{RSDAM}}^M)), \quad (3)$$

where $\text{Concat}(\cdot)$ represents the concatenation operation, $H_{\text{fusion}}(\cdot)$ indicates the function of feature fusion part which consists of a 1×1 convolution layer, a GELU [48] activation, and one 3×3 BSConv layer, and F_{fused} denotes the obtained fused feature. Finally, we employ a long skip connection across M RSDAMs to ease the residual learning, and the obtained $F_{\text{fused}} + F_0$ is further processed by the reconstruction block which is made up of a 3×3 convolution layer and a subpixel convolution layer [49] to yield the output SR image I_{SR} . The reconstruction block can be formulated as

$$I_{\text{SR}} = R(F_{\text{fused}} + F_0), \quad (4)$$

where $R(\cdot)$ is the function of the reconstruction block. To ensure fair comparison with previous SR methods, such as RFDN [13], FIWHN [16], and OSFFNet [18], we additionally optimize the model using the L1 loss function. Hence, we can formulate the loss function of our SDAN as

$$L(\Theta) = \frac{1}{N} \sum_{i=1}^N \|H_{\text{SDAN}}(I_{LR}^i) - I_{HR}^i\|_1, \quad (5)$$

Where $H_{\text{SDAN}}(\cdot)$ and Θ denote the function of the proposed SDAN and its learnable parameters, respectively. In addition, Adan [53] optimization algorithm, which combines the adaptive optimization, decoupling weight attenuation with modified Nesterov impulse, is adopted to optimize the network.

B. Star Distillation Module (SDM)

The self-attention mechanism has been widely used in recent years, leading to the element-wise multiplication as a new paradigm for fusing features from different subspaces. We call this paradigm "star operation" for simplicity. In the domains of computer vision (e.g., HorNet [54], VAN [40], FocalNet [55], etc.) and natural language processing (e.g., Monarch Mixer [56], Hyena Hierarchy [57], Mamba [58], etc.), star operation has demonstrated extensive applications and potent performance. StarNet is a straightforward yet effective prototype that Ma et al. [59] have proposed more recently. It demonstrates that the star operation can map inputs into HDNL feature spaces. Motivated by this, we propose a star distillation module (SDM) by incorporating the star operation with feature distillation structure based on channel splitting. As Figure 2 shows, SDM allows for information distillation in the HDNL feature spaces, which significantly enhance the learning for discriminative representation for lightweight image super-resolution (SR) task, leading to powerful reconstruction performance.

C. Multi-shape Multi-scale Large Kernel Attention (MM-LKA) module

We firstly revisit the large kernel attention (LKA) module in [40] before introducing the proposed multi-shape multi-scale large kernel attention (MM-LKA) in detail. For LKA, a 13×13 convolution can be decomposed into a 5×5 depth-wise convolution (DW-Conv5), a 5×5 depth-wise dilation convolution with dilation rate 3 (DW-D-Conv5), and a point-wise convolution (Conv1). Thus, we can formulate the process as

$$H_{\text{LKA}13}(F_{\text{in}}^i) = H_{\text{Conv1}} \left(H_{\text{DWDCov5}} \left(H_{\text{DWConv5}}(F_{\text{in}}^i) \right) \right) \otimes F_{\text{in}}^i, \quad (6)$$

where $H_{\text{LKA}13}(\cdot)$ denotes the process of LKA, F_{in}^i is the input feature of i -th LKA module, and \otimes represents element-wise product. Besides, $H_{\text{DWConv5}}(\cdot)$, $H_{\text{DWDCov5}}(\cdot)$, and

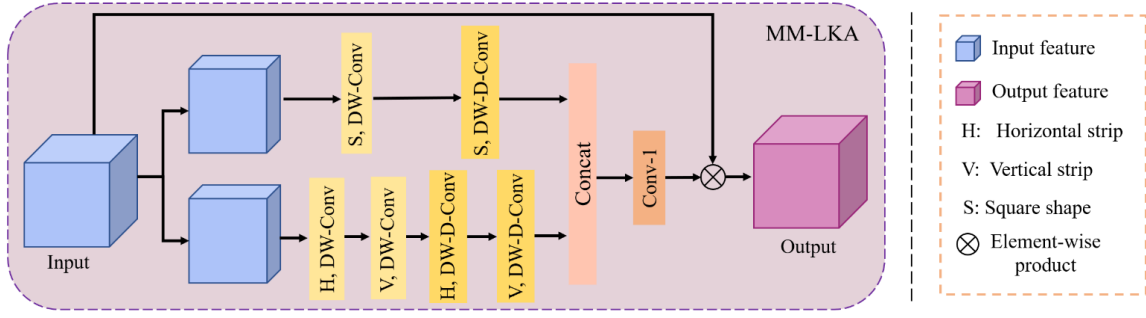


Fig. 3: The details of the proposed multi-shape multi-scale large kernel attention (MM-LKA).

$H_{Conv1}(\cdot)$ are the convolutional operations of DW-D-Conv5, DW-Conv5, and Conv1, respectively. We can observe that when the kernel sizes of the depth-wise separable convolutions in LKA increase, its complexity faces a quadratic increase in computational and memory footprints. And it neglects the learning of multi-shape multi-scale information for the long-range dependences.

To deal with the issues, we propose a multi-shape multi-scale large kernel attention (MM-LKA) which consists of one-dimensional (1D) depth-wise convolution, 1D depth-wise dilation convolution, two-dimensional (2D) depth-wise convolution, and 2D depth-wise dilation convolution. The details of the proposed MM-LKA are shown in Figure 3. Specifically, input features are divided into different groups which are refined respectively by the 1D convolutions and 2D convolutions, followed by a concatenation operation along channels. The concatenated feature maps are then fused by one 1×1 convolution layer to generate self-attention weights to reweight the prior input features F_{in}^i . Thus, MM-LKA possesses the learning ability for multi-shape multi-scale information for the long-range dependences while reducing the computational and memory footprints as the kernel sizes of the depth-wise separable convolutions increase, compared with LKA.

D. Residual star distillation attention module (RSDAM)

Integrating the proposed SDM and MM-LKA, we propose a residual star distillation attention module (RSDAM) and take it as the building block of the proposed SDAN. RSDAM can not only implement information distillation in HDNL feature spaces but also capture multi-shape multi-scale long-range dependencies, enhancing the discriminative representation learning.

In the k -th RSDAM, the input feature F_{RSDAM}^{k-1} is refined gradually. As Figure 4 shows, the process of star distillation module (SDM) can be expressed as

$$\begin{aligned} F_{d_1}, F_{s_1} &= D_1(F_{RSDAM}^{k-1}), S_1(F_{RSDAM}^{k-1}), \\ F_{d_2}, F_{s_2} &= D_2(F_{d_1}), S_2(F_{s_1}), \\ F_{d_3}, F_{s_3} &= D_3(F_{d_2}), S_3(F_{s_2}), \\ F_{d_4} &= D_4(F_{s_3}), \end{aligned} \quad (7)$$

where $D_i(\cdot)$ is the i -th 1×1 convolution layer of distillation operation, and $S_i(\cdot)$ denotes the corresponding operation of StarConv for feature refinement. F_{d_i} represents the obtained i -th distilled features and F_{s_i} is corresponding refined features.

Subsequently, all of the distilled features generated by 1×1 convolution layers in SDM are concatenated along the channel dimension, and we adopt a 1×1 convolution layer to fuse the concatenated features. The process can be expressed as

$$F_f = H_f(\text{Concat}(F_{d_1}, F_{d_2}, F_{d_3}, F_{d_4})), \quad (8)$$

where $H_f(\cdot)$ denotes the function of the 1×1 convolution layer, and F_f represents the its fused feature. Next, in order to further enhance the discriminative representation learning, we adopt the proposed MM-LKA module to capture multi-shape multi-scale long-range dependencies. We can formulate the process of MM-LKA as

$$F_{MM-LKA} = H_{MM-LKA}(F_f), \quad (9)$$

where $H_{MM-LKA}(\cdot)$, F_{MM-LKA} represent the function of MM-LKA, its refined features, respectively. Then, we use a 1×1 convolution layer to further refine F_{MM-LKA} , with a followed pixel normalization [60] module to facilitate stable model training. The process can be formulated as

$$F_{\text{normalized}} = \text{Norm}_{\text{pixel}}(\text{Conv}_{1 \times 1}(F_{MM-LKA})), \quad (10)$$

where $\text{Conv}_{1 \times 1}(\cdot)$, $\text{Norm}_{\text{pixel}}(\cdot)$, and $F_{\text{normalized}}$ represent the process of the 1×1 convolution layer, the function of pixel normalization, and the obtained normalized features, respectively. Finally, to enable the module to focus on residual learning, we make use of a long skip connection across the module. The process can be formulated as

$$F_{RSDAM}^k = F_{\text{normalized}} + F_{RSDAM}^{k-1}, \quad (11)$$

where F_{RSDAM}^k denotes the outcome of the k -th RSDAM.

IV. EXPERIMENTAL RESULTS

In this section, we firstly the introduce the experimental settings in detail, followed by a series of ablation experiments on SDAN to demonstrate its effectiveness. Next, a qualitative and quantitative comparison of our SDAN with other various lightweight SR methods is presented. Lastly, we conduct the complexity analysis of the proposed SDAN and discuss the limitations.

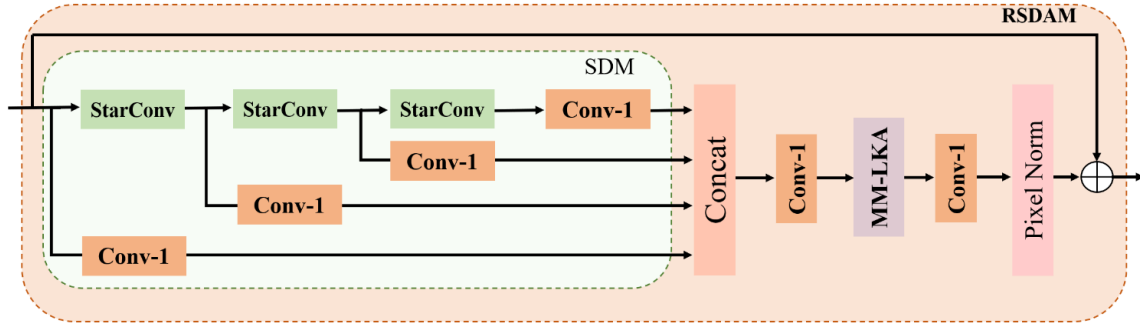


Fig. 4: The details of the proposed residual star distillation attention module (RSDAM) and its components: the proposed star distillation module (SDM) and the proposed MM-LKA. The Conv-1 and DW-Conv denote 1×1 convolution and depth-wise convolution, respectively.

A. Settings

To demonstrate the effectiveness and robustness of the proposed SDAN, following [18], we utilize the commonly used DF2K as the training dataset which consists of 800 images from DIV2K [61] and 2650 images from Flickr2K [5]. For fair comparison with previous SR methods, the corresponding LR images are produced via bicubic downsampling with scaling factors $\times 2$, $\times 3$ and $\times 4$. During training, 64×64 patches are generated by random cropping. The test datasets are made up of five common benchmark datasets: SET5 [62], SET14 [63], BSDS100 [64], URBAN100 [65], and MANGA109 [66]. The output results of the SR model are transformed to YCbCr space to calculate the peak signal-to-noise ratio (PSNR) and structural similarity index Measure (SSIM) [67] to quantitatively evaluate the model performance. Following [39], we optimize our SR model from scratch using the ADAN [53] optimizer with $\beta_1 = 0.98$, $\beta_2 = 0.92$ and $\beta_3 = 0.99$. The exponential moving average (EMA) is set to 0.999 to facilitate training. All experiments are conducted using the Pytorch [68] framework with one NVIDIA 3090 GPU. The learning rate is set to a constant 5×10^{-3} to train the network for 1×10^6 iterations.

B. Ablation studies

Break-down ablation. To evaluate the effectiveness of the proposed SDAN and the efficiency of its components, i.e., SDM and MM-LKA, we carry out a series of ablation experiments.

Initially, we use the DF2K dataset for $\times 4$ SR to train the model without the SDM and MM-LKA, using the tested performance of 32.21 dB PSNR on the Set5 ($\times 4$) dataset as the baseline.

The model with the SDM only is then trained and tested using the same datasets. The SDM has a strong feature extraction capability and can enhance reconstruction performance by capturing discriminative features via information distillation in the HDNL feature spaces, as verified by the test result which increases by 0.12 dB to 32.33 dB PSNR.

In order to validate the effectiveness of the MM-LKA, we repeat the same experiment on the model with MM-LKA only. The test result rises by 0.22 dB to 32.43 dB in comparison to

the baseline. Notably, MM-LKA can substantially improve the performance of the benchmark model in comparison to SDM.

Finally, the model with both SDM and MM-LKA is trained and tested under the same experimental settings to confirm the overall performance of SDAN. The obtained result reaches 32.54 dB, demonstrating the impressive performance of the suggested SDAN for lightweight SR. Table I shows all of the experimental results.

TABLE I: Ablation results from scratch on the Set5 dataset for $\times 4$ SR. The best result is **highlighted**.

Baseline	✓	✓	✓	✓
SDM	✗	✓	✗	✓
MM-LKA	✗	✗	✓	✓
PSNR/dB	32.21	32.33	32.43	32.54

Ablation of SDM. In order to validate the efficiency of the proposed star distillation module (SDM), we conduct corresponding experiments for $\times 3$ SR to show the selection of kernel size of depth-wise convolution in StarConv in SDM. In particular, the depth-wise convolutions in StarConv are separately implemented with different kernel sizes, ranging from 3 to 7. Considering the module complexity, we do not choose larger kernel sizes. Subsequently, under the same dataset and experimental setting, we carry out corresponding experiments to train the models, and test the trained models on Manga109 [66] dataset for $\times 3$ SR. The obtained experimental results are presented in Table II. It can be seen that the performance of the model improves as the kernel size increases, demonstrating the effectiveness of the proposed SDM.

TABLE II: Ablation results of SDM on the Manga109 dataset for $\times 3$ SR. The best result is **highlighted**.

kernel size (kz)	3	5	7
Network Params (K)	405	419	451
PSNR (dB)	34.16	34.20	34.25

Ablation of MM-LKA. To exploit the effect of different kernel sizes of square and strip depth-wise convolutions in the proposed multi-shape multi-scale large kernel attention (MM-LKA), convolutional kernels with different sizes are

adopted. Concretely, the kernel sizes of square depth-wise convolution and square dilated depth-wise convolution in MM-LKA vary from 5×5 to 7×7 , and those of strip depth-wise convolution and strip dilated depth-wise convolution are set to 7 or 11 to capture more contextual information. Then, we separately conduct corresponding experiments under the same training dataset and experimental setting for $\times 4$ SR, and we test the trained models on the Set5 ($\times 4$) dataset. Table III shows the detailed experimental results. We can see that as the square convolution kernel increases, the model achieves certain performance improvement, and the same trend goes for the strip depth-wise convolution. Moreover, models with both square depth-wise convolution and strip depth-wise convolution produce higher performance than single-shape convolution. Among them, the model which possesses 7×7 square convolution and strip depth-wise convolution with size of 11, yields the highest 32.54 dB PSNR. These experimental results indicate that the multi-shape multi-scale contextual information is crucial for efficient lightweight SR task.

TABLE III: Ablation results of the proposed MM-LKA on the Set5 dataset for $\times 4$ SR. The best result is **highlighted**.

square size	5×5	✓	✗	✗	✗	✗
	7×7	✗	✓	✓	✓	✗
strip size k	7	✓	✓	✗	✗	✗
	11	✗	✗	✓	✗	✓
Params/K	-	393	404	410	419	396
PSNR/dB	-	32.45	32.49	32.54	32.47	32.44

TABLE IV: Quantitative comparison of our SDAN with the heavy SR methods on benchmark datasets for $\times 4$ SR.

Method	Param	Set5	Set14	BSD100	Urban100
EDSR	43.1M	32.46dB	28.80dB	27.70dB	26.64dB
RDN	22.3M	32.47dB	28.80dB	27.72dB	26.60dB
RCAN	15.6M	32.63dB	28.87dB	27.77dB	26.82dB
DRN	9.8M	32.74dB	28.98dB	27.83dB	27.03dB
ERAN	8.02M	32.66dB	28.92dB	27.79dB	26.86dB
SDAN/ours	0.41M	32.54dB	28.81dB	27.72dB	26.65dB

C. Comparisons with other SR Methods

The effectiveness of our SDAN is further verified by quantitatively and visually comparing our experimental results for upscaling factors of $\times 2$, $\times 3$, and $\times 4$ with the results of other previous state-of-the-art lightweight SR networks, including SRCNN [1], VDSR [3], DRCN [10], DRRN [9], IDN [11], IMDN [12], RFDN [13], PFFN [14], CFDN [15], DIIN [69], FIWHN [16], EConvMixN [70], and OSFFNet [18].

PSNR/SSIM results. The quantitative evaluation results for $\times 2$, $\times 3$ and $\times 4$ lightweight SR are shown in Table IV. For $\times 2$ SR, in addition to achieving the majority of the top PSNR and SSIM values on five benchmark datasets, our SDAN has a minimum of 405 K model parameters compared with recent SR methods (PFFN, CFDN, FIWHN, and OSFFNet), demonstrating effectiveness of our SDAN. Using the same five benchmark datasets, our SDAN achieves the

maximum PSNR and SSIM for $\times 3$ SR with 407 K model parameters. Regarding $\times 4$ SR, our SDAN achieves all of the best quantitative results of PSNR and SSIM. Compared to previous lightweight state-of-the-art methods, it is evident that our SDAN can attain superiority for nearly all scaling factors (e.g., $\times 2$, $\times 3$, and $\times 4$). And, for larger amplification factors, the superiority of our method becomes more obvious. Overall, our method can produce superior reconstruction performance than other previous methods, as demonstrated quantitatively by the recorded experimental results. Furthermore, we compare the model complexity and performance of our SDAN for $\times 4$ SR on the benchmark datasets with the heavyweight state-of-the-art SR methods in Table V, including EDSR [49], RDN [7], RCAN [8], DRN [50], and ERAN [47]. On the Set14 and BSD100 datasets, our SDAN specifically achieves 28.81 dB and 27.72 dB respectively, and they are higher than corresponding values of the heavy network EDSR. Notably, the 43.1M parameters of EDSR are significantly more than the 0.41M parameters of our SDAN. Besides, it is noteworthy that our method obtains better performance than heavy network RDN on all four benchmark datasets (Set5, Set14, BSD100, and Urban100). Overall, our model requires at least 10 times less parameters than the heavier SR networks, yet it can still produce superior or comparable results, demonstrating its high efficiency. This attributes to the efficient information distillation via SDM module and the captured representative long-range dependencies by MM-LKA module.

Visual results. In Figure 5, different methods are visually compared on selected images from the five benchmark datasets, i.e., SET5, Set14, BSDS100, URBAN100, and MANGA109. For "woman.png" image in Set5 dataset, the original HR image has a lot of texture and contour information. The early bicubic algorithm produces the worst visual performance according to the these reconstruction results. In contrast, other CNN-based methods have produced better visual results. This trend also holds true for the quantitative results of PSNR and SSIM of these methods. For "ppt3.png" image in Set14, the early bicubic approach is still not a good reconstruction algorithm for SR because of its unstable trend, aliasing artifacts, and extensive blurring, while the visual results of other CNN-based techniques (such as RFDN, LBRN, and FIWHN) have significantly been improved. It can be seen that our SDAN can achieve sharper details and more complete outlines, especially for English words in the image. Regarding "148026.png" image in BSDS100 dataset, all of these methods produce shape distortions, yet the result of our method has minimal shape distortions, being more natural and clearer. In terms of "148026.png" in URBAN100 and "YumeiroCooking.png" in MANGA109, our SDAN yields superior results with sharper details and more natural textures, and the objects in the reconstructed images have the most complete shapes and contours. Overall, our SDAN can achieve the highest PSNR and SSIM for test images due to the extracted discriminative feature with effective information distillation and multi-shape multi-scale contextual information, and it produces the best visual perception among all these methods by recovering sharper details and more complete contours. All these results visually and quantitatively show

TABLE V: Quantitative results of our SDAN and previous state-of-the-art lightweight SR methods on benchmark datasets. The best and second-best results are **highlighted** and underlined, respectively.

Method	Years	Scale	Params	Set5 PSNR/SSIM	Set14 PSNR/SSIM	BSD100 PSNR/SSIM	Urban100 PSNR/SSIM	Manga109 PSNR/SSIM
Bicubic	-	-	-	33.66/0.9299	30.24/0.8688	29.56/0.8431	26.88/0.8403	30.80/0.9339
SRCNN	TPAMI15	-	8K	36.66/0.9542	32.45/0.9067	31.36/0.8879	29.50/0.8946	35.60/0.9663
VDSR	CVPR16	-	666K	37.53/0.9587	33.03/0.9124	31.90/0.8960	30.76/0.9140	37.22/0.9750
DRCN	CVPR16	-	1774K	37.63/0.9588	33.04/0.9118	31.85/0.8942	30.75/0.9133	37.55/0.9732
DRRN	CVPR17	-	298 K	37.74/0.9591	33.23/0.9136	32.05/0.8973	31.23/0.9188	37.88/0.9749
IDN	CVPR18	-	553K	37.83/0.9600	33.30/0.9148	32.08/0.8985	31.27/0.9196	38.01/0.9749
IMDN	MM19	-	694K	38.00/0.9605	33.63/0.9177	32.19/0.8996	32.17/0.9283	38.88/0.9774
RFDN	ECCV20	×2	534K	38.05/0.9606	33.68/0.9184	32.16/0.8994	32.12/0.9278	38.88/0.9773
PFFN	SPL24	-	572 K	<u>38.14/0.9608</u>	33.76/0.9190	32.29/0.9009	32.48/0.9317	-/-
CFDN	ICME24	-	820 K	<u>38.11/0.9613</u>	33.82/0.9199	32.26/0.9008	32.62/0.9328	-/-
EConvMixN	EAAI24	-	953 K	38.12/0.9609	33.70/0.9189	32.25/0.9007	32.44/0.9317	39.06/0.9778
OSFFNet	AAAI24	-	516K	38.11/0.9610	33.72/0.9190	32.29/0.9012	<u>32.67/0.9331</u>	<u>39.09/0.9780</u>
DIIN	TIM24	-	726K	38.06/0.9610	33.73/0.9189	32.20/0.8998	32.37/0.9301	38.95/0.9778
FIWHN	TMM24	-	705K	38.16/0.9613	33.73/0.9194	<u>32.27/0.9007</u>	32.75/0.9337	<u>39.07/0.9782</u>
SDAN	ours	-	405 K	<u>38.14/0.9611</u>	33.95/0.9203	32.29/0.9012	32.82/0.9344	39.21/0.9783
Bicubic	-	-	-	30.39/0.8682	27.55/0.7742	27.21/0.7385	24.46/0.7349	26.95/0.8556
SRCNN	TPAMI15	-	8K	32.75/0.9090	29.30/0.8215	28.41/0.7863	26.24/0.7989	30.48/0.9117
VDSR	CVPR16	-	666K	33.66/0.9213	29.77/0.8314	28.82/0.7976	27.14/0.8279	32.01/0.9340
DRCN	CVPR16	-	1774K	33.82/0.9226	29.76/0.8311	28.80/0.7963	27.15/0.8276	32.24/0.9343
DRRN	CVPR17	-	298 K	34.03/0.9244	29.96/0.8349	28.95/0.8004	27.53/0.8378	32.71/0.9379
IDN	CVPR18	-	553K	34.11/0.9253	29.99/0.8354	28.95/0.8013	27.42/0.8359	32.71/0.9381
IMDN	MM19	×3	703K	34.36/0.9270	30.32/0.8417	29.09/0.8046	28.17/0.8519	33.61/0.9445
RFDN	ECCV20	-	541K	34.41/0.9273	30.34/0.8420	29.09/0.8042	28.21/0.8525	33.67/0.9449
CFDN	ICME24	-	828 K	34.50/0.9286	30.41/0.8459	29.20/0.8081	<u>28.50/0.8587</u>	-/-
EConvMixN	EAAI24	-	965 K	34.56/0.9286	30.48/0.8452	29.19/0.8077	28.43/0.8586	33.92/0.9467
OSFFNet	AAAI24	-	524 K	<u>34.58/0.9287</u>	30.48/0.8450	<u>29.21/0.8080</u>	28.49/0.8595	<u>34.00/0.9472</u>
DIIN	TIM24	-	735K	34.48/0.9280	30.44/0.8436	29.13/0.8062	28.35/0.8551	33.87/0.9461
FIWHN	TMM24	-	713 K	34.50/0.9283	<u>30.50/0.8451</u>	29.19/0.8077	28.62/0.8607	<u>33.97/0.9472</u>
SDAN	ours	-	408 K	34.60/0.9289	30.52/0.8456	29.22/0.8085	28.62/0.8624	34.16/0.9479
Bicubic	-	-	-	28.42/0.8104	26.00/0.7027	25.96/0.6675	23.14/0.6577	24.89/0.7866
SRCNN	TPAMI15	-	8K	30.48/0.8626	27.50/0.7513	26.90/0.7101	24.52/0.7221	27.58/0.8555
VDSR	CVPR16	-	666K	31.35/0.8838	28.01/0.7674	27.29/0.7251	25.18/0.7524	28.83/0.8870
DRCN	CVPR16	-	1774K	31.53/0.8854	28.02/0.7670	27.23/0.7233	25.14/0.7510	28.93/0.8854
DRRN	CVPR17	-	298 K	31.68/0.8888	28.21/0.7720	27.38/0.7284	25.44/0.7638	29.45/0.8946
IDN	CVPR18	-	553K	31.82/0.8903	28.25/0.7730	27.41/0.7297	25.41/0.7632	29.41/0.8942
IMDN	MM19	×4	715K	32.21/0.8948	28.58/0.7811	27.56/0.7353	26.04/0.7838	30.45/0.9075
RFDN	ECCV20	-	550K	32.24/0.8952	28.61/0.7819	27.57/0.7360	26.11/0.7858	30.58/0.9089
PFFN	SPL24	-	572 K	32.35/0.8963	<u>28.77/0.7837</u>	<u>27.72/0.7390</u>	26.29/0.7903	-/-
CFDN	ICME24	-	838 K	<u>32.33/0.8981</u>	28.65/0.7855	<u>27.70/0.7407</u>	26.39/0.7957	-/-
EConvMixN	EAAI24	-	983 K	32.35/0.8972	28.69/0.7844	27.66/0.7398	26.30/0.7943	30.76/0.9125
OSFFNet	AAAI24	-	537K	<u>32.39/0.8976</u>	28.75/0.7852	27.66/0.7393	26.36/0.7950	30.84/0.9125
DIIN	TIM24	-	747K	32.35/0.8963	28.73/0.7842	27.63/0.7378	26.35/0.7920	30.81/0.9119
FIWHN	TMM24	-	725K	32.30/0.8967	28.76/0.7849	27.68/0.7400	26.57/0.7989	<u>30.93/0.9131</u>
SDAN	ours	-	410 K	32.54/0.8989	28.81/0.7866	27.74/0.7413	26.65/0.8031	31.13/0.9152

the effectiveness and superiority of the proposed SDAN.

D. Model Complexity Analysis

On the Urban100 dataset for ×2 SR, we further analyze and record the model complexity and reconstruction performance of different methods including IMDN [12], RFDN [13], CFIN [71], FIWHN [16], OSFFNet [18], and our SDAN. Specifically, we adopt the widely used evaluation metrics, model parameters and FLOPs [43] to show the model complexity, and we assume the SR output size to 1280× 720 to calculate FLOPs of these networks. Besides, we utilize the PSNR value to quantitatively evaluate the reconstruction quality of different outputs. The detailed results are shown in Table VI. Among these methods, FIWHN possesses the most parameters 705 K while achieving the second highest PSNR 32.75 dB. By contrast, our SDAN with the fewest parameters 405 K can obtain the highest PSNR 32.82 dB. As for the FLOPs,

OSFFNet has the fewest value 83.2 G and achieves 32.67 dB PSNR which is 0.15 dB lower than the 32.82 dB of our SDAN with 93.1 G FLOPs. These comparison results quantitatively show that our method is more efficient when dealing with image resolution degradation. The comparison of parameters and PSNR of these methods is visually illustrated in Figure 6, and we further show their comparison of FLOPs and PSNR in Figure 7.

E. Limitations

As shown in Figure 5, although our model obtains better visual results than our competitors in terms of lightweight single-image super-resolution, there is still a significant gap between our results and label HR images. The performance of the algorithm and the richness of the datasets should be further improved in future research.



Fig. 5: Visual comparisons for $\times 4$ SR with the BI model on the Set5, Set14, B100, Urban100 and Manga109 datasets. The best results are **highlighted**.

TABLE VI: Performance and model complexity comparison of different lightweight SR methods ($\times 2$ Urban100). The best results are **highlighted**.

Metric	IMDN	RFDN	CFIN	FIWHN	OSFFNet	SDAN
Years	MM19	ECCV20	TMM23	TMM24	AAAI24	ours
Paras/K	694	534	675	705	516	405
FLOPs/G	158.9	95.5	116.9	137.7	83.2	93.1
PSNR/dB	32.17	32.12	32.48	32.75	32.67	32.82

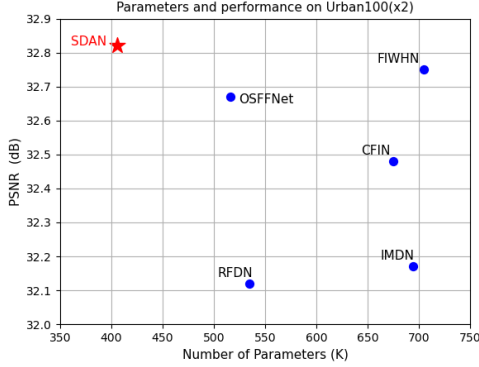


Fig. 6: Performance and the parameters of various lightweight SR methods on Urban100 ($\times 2$ SR).

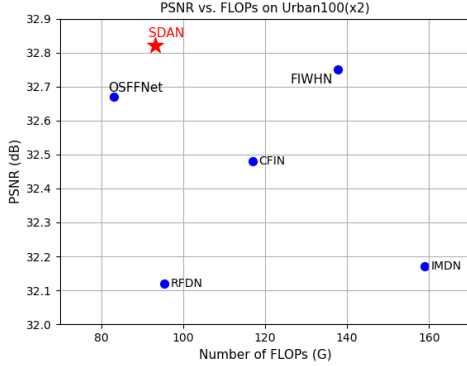


Fig. 7: Performance and the FLOPs of various lightweight SR methods on Urban100 ($\times 2$ SR).

V. CONCLUSION

In this study, we propose an efficient Star Distillation Attention Network (SDAN), a lightweight yet powerful framework for single-image super-resolution (SISR). The core innovation lies in the proposed Star Distillation Module (SDM) and the Multi-Shape Multi-Scale Large Kernel Attention (MM-LKA). SDM enhances discriminative representation learning via information distillation in the High-Dimensional Non-Linear (HDNL) feature spaces, and MM-LKA can capture multi-shape multi-scale contextual information effectively. By integrating SDM and MM-LKA, we further develop the Residual Star Distillation Attention Module (RSDAM) as the fundamental building block of SDAN, enabling hierarchical feature refinement while maintaining computational efficiency. Extensive experiments show the superiority of our method, demonstrating that SDAN with low model complexity achieves

superior performance in both quantitative metrics and visual quality.

ACKNOWLEDGMENTS

The authors would like to thank the reviewers for their insightful comments and useful suggestions.

REFERENCES

- [1] C. Dong, C. C. Loy, K. He, and X. Tang, “Image super-resolution using deep convolutional networks,” *IEEE transactions on pattern analysis and machine intelligence*, vol. 38, no. 2, pp. 295–307, 2015.
- [2] L. Zhang and X. Wu, “An edge-guided image interpolation algorithm via directional filtering and data fusion,” *IEEE transactions on Image Processing*, vol. 15, no. 8, pp. 2226–2238, 2006.
- [3] J. Kim, J. K. Lee, and K. M. Lee, “Accurate image super-resolution using very deep convolutional networks,” in *Proceedings of the IEEE conference on computer vision and pattern recognition*, 2016, pp. 1646–1654.
- [4] K. He, X. Zhang, S. Ren, and J. Sun, “Deep residual learning for image recognition,” in *Proceedings of the IEEE conference on computer vision and pattern recognition*, 2016, pp. 770–778.
- [5] B. Lim, S. Son, H. Kim, S. Nah, and K. Mu Lee, “Enhanced deep residual networks for single image super-resolution,” in *Proceedings of the IEEE conference on computer vision and pattern recognition workshops*, 2017, pp. 136–144.
- [6] G. Huang, Z. Liu, L. Van Der Maaten, and K. Q. Weinberger, “Densely connected convolutional networks,” in *Proceedings of the IEEE conference on computer vision and pattern recognition*, 2017, pp. 4700–4708.
- [7] Y. Zhang, Y. Tian, Y. Kong, B. Zhong, and Y. Fu, “Residual dense network for image super-resolution,” in *Proceedings of the IEEE conference on computer vision and pattern recognition*, 2018, pp. 2472–2481.
- [8] Y. Zhang, K. Li, K. Li, L. Wang, B. Zhong, and Y. Fu, “Image super-resolution using very deep residual channel attention networks,” in *Proceedings of the European conference on computer vision (ECCV)*, 2018, pp. 286–301.
- [9] Y. Tai, J. Yang, and X. Liu, “Image super-resolution via deep recursive residual network,” in *Proceedings of the IEEE conference on computer vision and pattern recognition*, 2017, pp. 3147–3155.
- [10] J. Kim, J. K. Lee, and K. M. Lee, “Deeply-recursive convolutional network for image super-resolution,” in

- Proceedings of the IEEE conference on computer vision and pattern recognition*, 2016, pp. 1637–1645.
- [11] Z. Hui, X. Wang, and X. Gao, “Fast and accurate single image super-resolution via information distillation network,” in *Proceedings of the IEEE conference on computer vision and pattern recognition*, 2018, pp. 723–731.
 - [12] Z. Hui, X. Gao, Y. Yang, and X. Wang, “Lightweight image super-resolution with information multi-distillation network,” in *Proceedings of the 27th acm international conference on multimedia*, 2019, pp. 2024–2032.
 - [13] J. Liu, J. Tang, and G. Wu, “Residual feature distillation network for lightweight image super-resolution,” in *Computer vision—ECCV 2020 workshops: Glasgow, UK, August 23–28, 2020, proceedings, part III 16*. Springer, 2020, pp. 41–55.
 - [14] B. Liu, X. Ning, S. Ma, and X. Lian, “A lightweight pyramid feature fusion network for single image super-resolution reconstruction,” *IEEE Signal Processing Letters*, 2024.
 - [15] X. Wu, L. Chen, M. Tan, and Y. Wu, “Convolutional modulation feature distillation network for image super-resolution,” in *2024 IEEE International Conference on Multimedia and Expo (ICME)*. IEEE, 2024, pp. 1–6.
 - [16] W. Li, J. Li, G. Gao, W. Deng, J. Yang, G.-J. Qi, and C.-W. Lin, “Efficient image super-resolution with feature interaction weighted hybrid network,” *IEEE Transactions on Multimedia*, 2024.
 - [17] J. Li and Y. Ke, “Hybrid convolution-transformer for lightweight single image super-resolution,” in *ICASSP 2024-2024 IEEE International Conference on Acoustics, Speech and Signal Processing (ICASSP)*. IEEE, 2024, pp. 2395–2399.
 - [18] Y. Wang and T. Zhang, “Osfnet: Omni-stage feature fusion network for lightweight image super-resolution,” in *Proceedings of the AAAI conference on artificial intelligence*, vol. 38, no. 6, 2024, pp. 5660–5668.
 - [19] A. Vaswani, N. Shazeer, N. Parmar, J. Uszkoreit, L. Jones, A. N. Gomez, Ł. Kaiser, and I. Polosukhin, “Attention is all you need,” *Advances in neural information processing systems*, vol. 30, 2017.
 - [20] J. Hu, L. Shen, and G. Sun, “Squeeze-and-excitation networks,” in *Proceedings of the IEEE conference on computer vision and pattern recognition*, 2018, pp. 7132–7141.
 - [21] B. N. Xia, Y. Gong, Y. Zhang, and C. Poellabauer, “Second-order non-local attention networks for person re-identification,” in *Proceedings of the IEEE/CVF international conference on computer vision*, 2019, pp. 3760–3769.
 - [22] A. Dosovitskiy, L. Beyer, A. Kolesnikov, D. Weissenborn, X. Zhai, T. Unterthiner, M. Dehghani, M. Minderer, G. Heigold, S. Gelly *et al.*, “An image is worth 16x16 words: Transformers for image recognition at scale,” *arXiv preprint arXiv:2010.11929*, 2020.
 - [23] Z. Liu, Y. Lin, Y. Cao, H. Hu, Y. Wei, Z. Zhang, S. Lin, and B. Guo, “Swin transformer: Hierarchical vision transformer using shifted windows,” in *Proceedings of the IEEE/CVF international conference on computer vision*, 2021, pp. 10012–10022.
 - [24] S. Sun, X. Yue, H. Zhao, P. H. Torr, and S. Bai, “Patch-based separable transformer for visual recognition,” *IEEE transactions on pattern analysis and machine intelligence*, vol. 45, no. 7, pp. 9241–9247, 2022.
 - [25] K. W. Lau, L.-M. Po, and Y. A. U. Rehman, “Large separable kernel attention: Rethinking the large kernel attention design in cnn,” *Expert Systems with Applications*, vol. 236, p. 121352, 2024.
 - [26] X. Wang, Z. Cai, D. Gao, and N. Vasconcelos, “Towards universal object detection by domain attention,” in *Proceedings of the IEEE/CVF conference on computer vision and pattern recognition*, 2019, pp. 7289–7298.
 - [27] Q. Fan, W. Zhuo, C.-K. Tang, and Y.-W. Tai, “Few-shot object detection with attention-rpn and multi-relation detector,” in *Proceedings of the IEEE/CVF conference on computer vision and pattern recognition*, 2020, pp. 4013–4022.
 - [28] C. Symeonidis, I. Mademlis, I. Pitas, and N. Nikolaidis, “Neural attention-driven non-maximum suppression for person detection,” *IEEE transactions on image processing*, vol. 32, pp. 2454–2467, 2023.
 - [29] L. Zhang and K. Ma, “Structured knowledge distillation for accurate and efficient object detection,” *IEEE Transactions on Pattern Analysis and Machine Intelligence*, vol. 45, no. 12, pp. 15 706–15 724, 2023.
 - [30] P.-T. Jiang, L.-H. Han, Q. Hou, M.-M. Cheng, and Y. Wei, “Online attention accumulation for weakly supervised semantic segmentation,” *IEEE Transactions on Pattern Analysis and Machine Intelligence*, vol. 44, no. 10, pp. 7062–7077, 2021.
 - [31] X. He, J. Liu, W. Wang, and H. Lu, “An efficient sampling-based attention network for semantic segmentation,” *IEEE Transactions on Image Processing*, vol. 31, pp. 2850–2863, 2022.
 - [32] H. Shi, M. Hayat, and J. Cai, “Transformer scale gate for semantic segmentation,” in *Proceedings of the IEEE/CVF conference on computer vision and pattern recognition*, 2023, pp. 3051–3060.
 - [33] Z. Lu, S. He, D. Li, Y.-Z. Song, and T. Xiang, “Prediction calibration for generalized few-shot semantic segmentation,” *IEEE transactions on image processing*, vol. 32, pp. 3311–3323, 2023.
 - [34] F. Zhang, A. Panahi, and G. Gao, “Fsanet: Frequency self-attention for semantic segmentation,” *IEEE Transactions on Image Processing*, vol. 32, pp. 4757–4772, 2023.
 - [35] F. Hao, J. Du, W. Liang, J. Xu, and X. Xu, “Towards context-aware convolutional network for image restoration,” *Knowledge-Based Systems*, p. 113579, 2025.
 - [36] X. Luo, Y. Qu, Y. Xie, Y. Zhang, C. Li, and Y. Fu, “Lattice network for lightweight image restoration,” *IEEE Transactions on Pattern Analysis and Machine Intelligence*, vol. 45, no. 4, pp. 4826–4842, 2022.
 - [37] H. Feng, L. Wang, Y. Li, and A. Du, “Lkasr: Large kernel attention for lightweight image super-resolution,” *Knowledge-Based Systems*, vol. 252, p. 109376, 2022.

- [38] Y. Hu, Y. Huang, and K. Zhang, “Multi-scale information distillation network for efficient image super-resolution,” *Knowledge-Based Systems*, vol. 275, p. 110718, 2023.
- [39] C. Xie, X. Zhang, L. Li, H. Meng, T. Zhang, T. Li, and X. Zhao, “Large kernel distillation network for efficient single image super-resolution,” in *Proceedings of the IEEE/CVF conference on computer vision and pattern recognition*, 2023, pp. 1283–1292.
- [40] M.-H. Guo, C.-Z. Lu, Z.-N. Liu, M.-M. Cheng, and S.-M. Hu, “Visual attention network,” *Computational visual media*, vol. 9, no. 4, pp. 733–752, 2023.
- [41] F. Hao, J. Wu, H. Lu, J. Du, J. Xu, and X. Xu, “Large coordinate kernel attention network for lightweight image super-resolution,” *arXiv preprint arXiv:2405.09353*, 2024.
- [42] K. Zhang, S. Gu, R. Timofte, Z. Hui, X. Wang, X. Gao, D. Xiong, S. Liu, R. Gang, N. Nan *et al.*, “Aim 2019 challenge on constrained super-resolution: Methods and results,” in *2019 IEEE/CVF International Conference on Computer Vision Workshop (ICCVW)*. IEEE, 2019, pp. 3565–3574.
- [43] Q. Wang, B. Wu, P. Zhu, P. Li, W. Zuo, and Q. Hu, “Eca-net: Efficient channel attention for deep convolutional neural networks,” in *Proceedings of the IEEE/CVF conference on computer vision and pattern recognition*, 2020, pp. 11 534–11 542.
- [44] Q.-L. Zhang and Y.-B. Yang, “Sa-net: Shuffle attention for deep convolutional neural networks,” in *ICASSP 2021-2021 IEEE International Conference on Acoustics, Speech and Signal Processing (ICASSP)*. IEEE, 2021, pp. 2235–2239.
- [45] G. Gao, W. Li, J. Li, F. Wu, H. Lu, and Y. Yu, “Feature distillation interaction weighting network for lightweight image super-resolution,” in *Proceedings of the AAAI conference on artificial intelligence*, vol. 36, no. 1, 2022, pp. 661–669.
- [46] N. Ahn, B. Kang, and K.-A. Sohn, “Fast, accurate, and lightweight super-resolution with cascading residual network,” in *Proceedings of the European conference on computer vision (ECCV)*, 2018, pp. 252–268.
- [47] F. Hao, T. Zhang, L. Zhao, and Y. Tang, “Efficient residual attention network for single image super-resolution,” *Applied Intelligence*, vol. 52, no. 1, pp. 652–661, 2022.
- [48] D. Hendrycks and K. Gimpel, “Gaussian error linear units (gelus),” *arXiv preprint arXiv:1606.08415*, 2016.
- [49] W. Shi, J. Caballero, F. Huszár, J. Totz, A. P. Aitken, R. Bishop, D. Rueckert, and Z. Wang, “Real-time single image and video super-resolution using an efficient sub-pixel convolutional neural network,” in *Proceedings of the IEEE conference on computer vision and pattern recognition*, 2016, pp. 1874–1883.
- [50] Y. Guo, J. Chen, J. Wang, Q. Chen, J. Cao, Z. Deng, Y. Xu, and M. Tan, “Closed-loop matters: Dual regression networks for single image super-resolution,” in *Proceedings of the IEEE/CVF conference on computer vision and pattern recognition*, 2020, pp. 5407–5416.
- [51] X. Chu, B. Zhang, H. Ma, R. Xu, and Q. Li, “Fast, accurate and lightweight super-resolution with neural architecture search,” in *2020 25th International conference on pattern recognition (ICPR)*. IEEE, 2021, pp. 59–64.
- [52] G. Cheng, A. Matsune, H. Du, X. Liu, and S. Zhan, “Exploring more diverse network architectures for single image super-resolution,” *Knowledge-Based Systems*, vol. 235, p. 107648, 2022.
- [53] X. Xie, P. Zhou, H. Li, Z. Lin, and S. Yan, “Adan: Adaptive nesterov momentum algorithm for faster optimizing deep models,” *IEEE Transactions on Pattern Analysis and Machine Intelligence*, 2024.
- [54] Y. Rao, W. Zhao, Y. Tang, J. Zhou, S. N. Lim, and J. Lu, “Hornet: Efficient high-order spatial interactions with recursive gated convolutions,” *Advances in Neural Information Processing Systems*, vol. 35, pp. 10 353–10 366, 2022.
- [55] J. Yang, C. Li, X. Dai, and J. Gao, “Focal modulation networks,” *Advances in Neural Information Processing Systems*, vol. 35, pp. 4203–4217, 2022.
- [56] D. Fu, S. Arora, J. Grogan, I. Johnson, E. S. Eyuboglu, A. Thomas, B. Spector, M. Poli, A. Rudra, and C. Ré, “Monarch mixer: A simple sub-quadratic gemm-based architecture,” *Advances in Neural Information Processing Systems*, vol. 36, pp. 77 546–77 603, 2023.
- [57] M. Poli, S. Massaroli, E. Nguyen, D. Y. Fu, T. Dao, S. Baccus, Y. Bengio, S. Ermon, and C. Ré, “Hyena hierarchy: Towards larger convolutional language models,” in *International Conference on Machine Learning*. PMLR, 2023, pp. 28 043–28 078.
- [58] A. Gu and T. Dao, “Mamba: Linear-time sequence modeling with selective state spaces,” *arXiv preprint arXiv:2312.00752*, 2023.
- [59] X. Ma, X. Dai, Y. Bai, Y. Wang, and Y. Fu, “Rewrite the stars,” in *Proceedings of the IEEE/CVF Conference on Computer Vision and Pattern Recognition*, 2024, pp. 5694–5703.
- [60] L. Zhou, H. Cai, J. Gu, Z. Li, Y. Liu, X. Chen, Y. Qiao, and C. Dong, “Efficient image super-resolution using vast-receptive-field attention,” in *European conference on computer vision*. Springer, 2022, pp. 256–272.
- [61] R. Timofte, E. Agustsson, L. Van Gool, M.-H. Yang, and L. Zhang, “Ntire 2017 challenge on single image super-resolution: Methods and results,” in *Proceedings of the IEEE conference on computer vision and pattern recognition workshops*, 2017, pp. 114–125.
- [62] M. Bevilacqua, A. Roumy, C. Guillemot, and M. L. Alberi-Morel, “Low-complexity single-image super-resolution based on nonnegative neighbor embedding,” 2012.
- [63] R. Zeyde, M. Elad, and M. Protter, “On single image scale-up using sparse-representations,” in *International conference on curves and surfaces*. Springer, 2010, pp. 711–730.
- [64] P. Arbelaez, M. Maire, C. Fowlkes, and J. Malik, “Contour detection and hierarchical image segmentation,” *IEEE transactions on pattern analysis and machine intelligence*, vol. 33, no. 5, pp. 898–916, 2010.
- [65] J.-B. Huang, A. Singh, and N. Ahuja, “Single image super-resolution from transformed self-exemplars,” in

Proceedings of the IEEE conference on computer vision and pattern recognition, 2015, pp. 5197–5206.

- [66] Y. Matsui, K. Ito, Y. Aramaki, A. Fujimoto, T. Ogawa, T. Yamasaki, and K. Aizawa, “Sketch-based manga retrieval using manga109 dataset,” *Multimedia tools and applications*, vol. 76, pp. 21 811–21 838, 2017.
- [67] Z. Wang, A. C. Bovik, H. R. Sheikh, and E. P. Simoncelli, “Image quality assessment: from error visibility to structural similarity,” *IEEE transactions on image processing*, vol. 13, no. 4, pp. 600–612, 2004.
- [68] A. Paszke, S. Gross, S. Chintala, G. Chanan, E. Yang, Z. DeVito, Z. Lin, A. Desmaison, L. Antiga, and A. Lerer, “Automatic differentiation in pytorch,” 2017.
- [69] H. Jin, G. Gao, J. Li, Z. Guo, and Y. Yu, “Efficient dual-branch information interaction network for lightweight image super-resolution,” *IEEE Transactions on Instrumentation and Measurement*, 2024.
- [70] G. Gendy, N. Sabor, and G. He, “Lightweight image super-resolution network based on extended convolution mixer,” *Engineering Applications of Artificial Intelligence*, vol. 133, p. 108069, 2024.
- [71] W. Li, J. Li, G. Gao, W. Deng, J. Zhou, J. Yang, and G.-J. Qi, “Cross-receptive focused inference network for lightweight image super-resolution,” *IEEE Transactions on Multimedia*, vol. 26, pp. 864–877, 2023.